forests

MDPI

Article

Initial Soil Moisture Threshold Influences Rainfall–Runoff Processes of Mixed-Forest Catchment: A Case Study of the Dabie Mountains

Yu Mei [1,2], Qinghe Zhao [1,2,3,4,*], Di Wu [1,2], Tingting Wang [1,2], Luwei Zhang [1,2] and Shengyan Ding [1,2,3,*]

[1] Faculty of Geographical Science and Engineering, College of Geographical Sciences, Henan University, Zhengzhou 450046, China; meiyu@henu.edu.cn (Y.M.); wdi@henu.edu.cn (D.W.); ttwang@henu.edu.cn (T.W.); zhangluwei@henu.edu.cn (L.Z.)
[2] Key Laboratory of Geospatial Technology for the Middle and Lower Yellow River Regions, Henan University, Ministry of Education, Kaifeng 475004, China
[3] Henan Dabieshan National Field Observation and Research Station of Forest Ecosystem, Xinyang 464039, China
[4] Xiaoqinling Ecological Restoration Field Observation and Research Station of the Yellow River Basin, Henan University, Kaifeng 475004, China
* Correspondence: zhaoqinghe@henu.edu.cn (Q.Z.); syding@henu.edu.cn (S.D.)

Abstract

Initial soil moisture (ISM) represents the soil moisture condition before a rainfall event and is an important factor associated with rainfall and runoff responses in forested catchments. However, it remains unclear whether this nonlinearity can be characterized by distinct ISM thresholds and whether the dominant controls of runoff coefficient (RC) and specific peak discharge (SPD) differ between pre-threshold and post-threshold ISM states. To address this issue, this study analyzed 27 rainfall events monitored in mixed-forest catchments of the Dabie Mountains from 2024 to 2026. A random forest model combined with SHapley additive exPlanations (SHAP) and partial dependence plots (PDPs) was used to simulate RC and SPD, identify ISM thresholds, and compare state-dependent dominant factors and interactions. The results showed that the SHAP-derived ISM thresholds were 18.3% for RC and 19.2% for SPD. For RC, ISM remained the dominant factor in both ISM states. In the pre-threshold state, rainfall intensity (RI) and net precipitation (NP) were the main secondary factors, with RI × ISM and NP × ISM as the leading interactions. In the post-threshold state, temperature and evaporation (Evap) became more important, and the leading interactions shifted to Evap × ISM and ISM × atmospheric pressure. For SPD, the dominant factors in the pre-threshold state were RI, NP, and ISM, with NP × RI and RI × ISM as the main interactions. In the post-threshold state, ISM became the leading factor, wind speed and RI also remained important, and ISM × wind speed and RI × ISM were the main interactions. These findings indicate that event-scale rainfall–runoff responses in mixed-forest catchments are strongly dependent on ISM state, and that ISM thresholds can provide useful boundaries for distinguishing state-dependent runoff-control patterns.

Keywords: initial soil moisture; net precipitation; rainfall–runoff processes; threshold; mixed-forest

Check for updates

Academic Editor: Carlos R. Mello

Received: 24 July 2026
Revised: 17 August 2026
Accepted: 17 August 2026
Published: 20 August 2026

1. Introduction

Understanding rainfall–runoff processes in forested catchments is important for flood-risk assessment, as floods account for up to 35%–40% of weather-related disasters worldwide, while weather-, climate-, and water-related hazards caused approximately USD 4.3 trillion in reported economic losses between 1970 and 2021 [1,2]. Rainfall–runoff processes in forested catchments are influenced not only by rainfall input but also by canopy-mediated rainfall redistribution and initial soil moisture conditions (ISM) [3,4]. Forest canopies modify net precipitation (NP) through interception, throughfall, and stemflow, while infiltration, evapotranspiration, and soil water storage further affect the conversion of rainfall into runoff [5,6]. As a result, similar rainfall events may produce different runoff coefficients and peak discharges under different ISM conditions within the same catchment [7,8]. This complexity may be more pronounced in mixed-forest catchments, where heterogeneous canopy structures and spatially variable soil moisture conditions can increase the variability of rainfall–runoff processes [9,10].

Among the factors affecting event-scale rainfall–runoff processes, ISM is a key state variable because it reflects antecedent soil water storage [11,12]. Under relatively dry conditions, rainfall may first replenish soil-water deficits, thereby reducing runoff generation and specific peak discharge (SPD) [13,14]. Under wetter antecedent conditions, the remaining storage capacity is lower, and hydrological connectivity within the catchment may be enhanced [12,15], allowing a larger proportion of rainfall to be converted to runoff [16,17]. Therefore, ISM can influence both runoff conversion efficiency and SPD formation, although these two runoff processes may not be influenced in exactly the same way [18,19].

Previous studies conducted under contrasting climatic, geological, and vegetation conditions have shown that event-scale rainfall–runoff responses in forested catchments may change nonlinearly with antecedent wetness conditions [20,21]. In the Bongsunsa watershed, South Korea, a classification and regression tree analysis identified both rainfall and soil-moisture thresholds associated with changes in runoff-generation behavior [20]. In Mediterranean forested headwater catchments in the southern Sierra Nevada, California, USA, runoff thresholds and flow pathways were found to be jointly affected by rainfall characteristics and antecedent soil-moisture conditions [22]. Similar nonlinear and threshold-dependent rainfall–runoff responses have also been reported on a karst hillslope in the peak-cluster depression region of southwestern China [23]. In the Coweeta forested headwater catchment in the southern Appalachian Mountains, USA, ISM and storm characteristics were likewise shown to jointly influence soil-moisture responses and runoff generation [24]. Across these different settings, rainfall under low-ISM conditions is more likely to replenish soil-water deficits before contributing substantially to runoff [2,22], whereas reduced storage capacity under high-ISM conditions can promote more efficient rainfall-to-runoff conversion and stronger peak-flow responses [23,25]. Related studies in afforested catchments in Great Britain [21], a cloud forest in central Taiwan [22], the Three-River Source region of China [24], and vegetation-restored catchments of the Chinese Loess Plateau [26] further indicate that forest structure, canopy processes, land-cover change, and regional hydroclimatic conditions can modify rainfall–runoff responses.

Despite these advances, previous threshold-oriented studies have primarily focused on rainfall amount or rainfall intensity as triggers of runoff activation and transitions in runoff-generation mechanisms [20,23,26,27]. Even when ISM has been considered, it has often been used as an antecedent wetness descriptor for explaining variations in runoff magnitude or improving soil moisture–runoff coupling, rather than as a state variable for distinguishing runoff-control patterns before and after a threshold [25,28]. Machine-learning models have increasingly been applied to identify nonlinear controls of watershed streamflow variability [5], while SHAP-based frameworks have been used to quantify and interpret the contributions of environmental factors to hydrological and flood responses [29]. However, it remains unclear whether SHAP-derived ISM transition points can distinguish changes in dominant controls and interactions between pre-threshold and post-threshold states, and whether these changes are consistent for event-integrated runoff conversion and peak-flow formation. To address this gap, rainfall–runoff responses were represented by two complementary event-scale metrics: runoff coefficient (RC), which reflects rainfall-to-runoff conversion efficiency, and SPD, which represents peak-flow formation during rainfall events [10,28]. Comparing the dominant controls and interaction structures of RC and SPD across ISM threshold states can reveal whether different components of rainfall–runoff responses exhibit similar or distinct state-dependent patterns in forested catchments [30,31].

A reliable analysis of rainfall–runoff relationships requires not only consideration of antecedent wetness conditions such as ISM, but also an appropriate representation of rainfall input reaching the forest floor [32,33]. Total precipitation and rainfall intensity are commonly used to characterize rainfall forcing [17,28]. However, precipitation is modified by canopy interception and redistribution before reaching the soil surface [22,34]. NP, which comprises throughfall, stemflow, and rainfall reaching canopy gaps, therefore represents canopy-adjusted event water input reaching the forest floor. In the present study, NP was included together with ISM and meteorological variables to examine predictor–response relationships for RC and SPD. Because total precipitation was not included as an alternative predictor in the RF models, the importance of NP is interpreted only within the predictor set analyzed and does not demonstrate that NP has greater predictive capability than total precipitation [35].

Against this background, this study investigated 27 rainfall events from three monitored mixed-forest catchments within the Xiangchagou watershed of the Dabie Mountains, using NP, ISM, and event-based runoff observations. An interpretable machine-learning framework integrating RF, SHapley additive exPlanations (SHAP), and partial dependence plots (PDPs) was used to identify ISM thresholds for RC and SPD, and to compare the dominant factors associated with RC and SPD between pre-threshold and post-threshold ISM states. Specifically, this study aimed to perform the following: (1) evaluate the relative importance and nonlinear effects of ISM, NP, and meteorological factors on RC and SPD at the event scale; (2) identify SHAP-derived ISM thresholds in the response relationships of RC and SPD; and (3) compare the dominant controls of RC and SPD between pre-threshold and post-threshold ISM states. By distinguishing differences in runoff-control patterns under different ISM states, this study provides useful information for improving event-scale runoff prediction in mixed-forest catchments.

2. Materials and Methods

2.1. Study Area

This study was conducted in the Xiangchagou watershed (3.66 km^2), located on the southern slopes of the Jigong Mountain National Nature Reserve in the Dabie Mountains, Henan Province, China (Figure 1). The watershed lies within the north–south climatic transitional zone of China along the "Qinling-Huaihe line", characterized by mountainous and hilly terrain under a humid subtropical monsoon climate. The mean annual temperature is 15.2 °C, and the average annual precipitation is 1119 mm, with the majority of rainfall occurring between April and October [36,37]. During intense rainfall events, the watershed responds rapidly and can generate distinct flood peaks. The watershed is predominantly covered by Cambisols according to the FAO soil classification system, locally characterized by yellow-brown sandy loam soils. These soils have developed mainly from the weathering of mixed granite and composite-granite batholiths and are generally shallow and acidic. The shallow weathered mantle and locally exposed or fractured bedrock may limit subsurface water storage and facilitate rapid lateral water transfer under wet conditions. Elevations range from 175 to 516 m [38,39]. Since the 1950s, intensive human activities, particularly deforestation and land cultivation, have caused significant degradation of the original forest cover, leaving the area primarily covered by secondary forests. Due to the region's transitional climate, the vegetation includes both warm–temperate and subtropical forest types, with deciduous broadleaf trees and conifers. The dominant species include *Quercus acutissima*, *Quercus variabilis*, and *Cunninghamia lanceolata*.

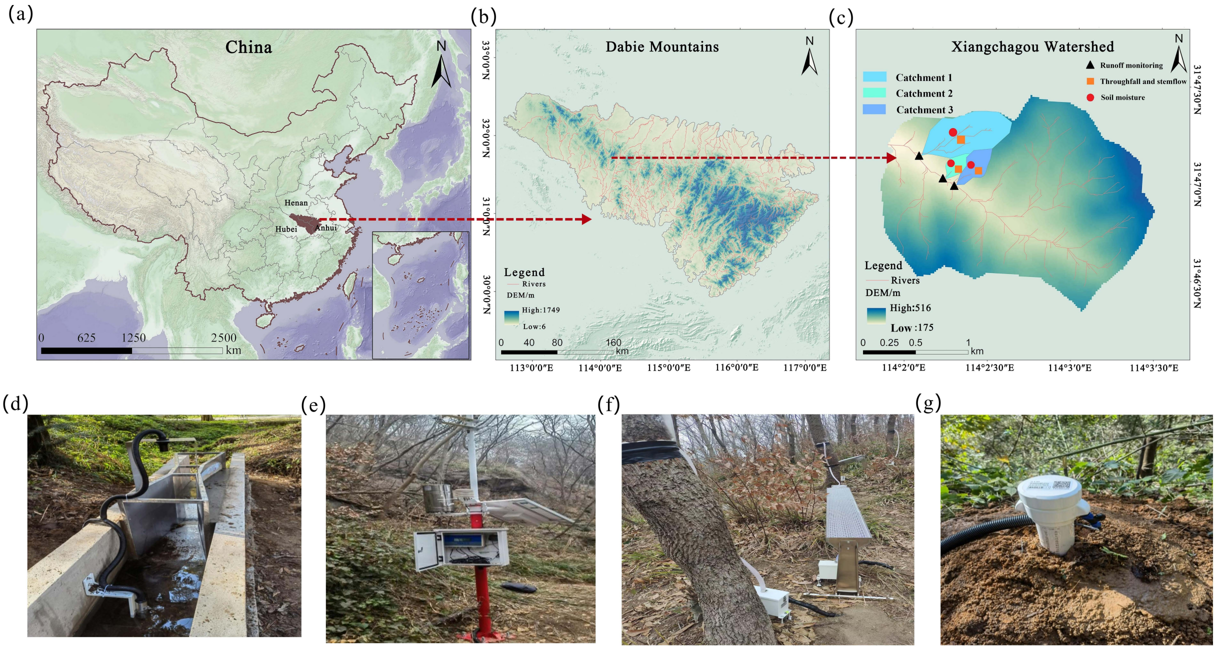

Figure 1. Location of the study area and field monitoring setup. (**a**) Location of the Dabie Mountains in China; (**b**) location of the study area in the Dabie Mountains; (**c**) location of the Xiangchagou watershed and distribution of the experimental catchments and monitoring sites; (**d**) runoff monitoring facility; (**e**) micro-meteorological station; (**f**) throughfall and stemflow monitoring equipment; and (**g**) soil moisture sensor.

Within the Xiangchagou watershed, three catchments were selected for runoff monitoring. The catchments were delineated according to their natural topographic drainage boundaries and the locations of the runoff-monitoring outlets. The outlet of each catchment corresponded to the monitoring cross-section controlling its upstream drainage area. The three catchments were selected because they had clearly defined drainage boundaries and single runoff-concentration outlets suitable for continuous monitoring, while also exhibiting broadly comparable topographic and vegetation conditions and limited direct human disturbance. All three catchments are covered by mixed deciduous broadleaf and coniferous forests and have similar slope gradients and aspects. Their main topographic and vegetation characteristics are summarized in Table 1. The monitoring period extended from January 2024 to January 2026, during which a total of 27 events with complete rainfall–runoff records were identified. For each rainfall event, runoff responses were recorded separately in the three monitored catchments.

Table 1. Topographic and vegetation characteristics of the three monitored catchments.

Characteristic	Catchment 1	Catchment 2	Catchment 3
Area (km^2)	0.26	0.03	0.06
Mean elevation	233	223	273
Mean slope (degrees)	28.6	21.5	23.8
Dominant aspect	South	South	South
Canopy closure (%)	93	90	88
Dominant tree species	*Quercus acutissima* C *Quercus variabilis* B	*Quercus acutissima* C *Castanea mollissima* B	*Pinus massoniana* L. *Quercus acutissima* C

2.2. Field Monitoring

2.2.1. Rainfall, Throughfall, Stemflow and NP Monitoring

A JZ-HB-9 micro-meteorological station (Beijing Jiuzhou Shengxin Technology Co., Ltd., Beijing, China) was installed in each catchment. The station was operated according to the manufacturer's technical specifications, and no additional field calibration or intercomparison with reference instruments was conducted during this study. Monitoring records were screened for completeness, temporal continuity, and physically implausible values before analysis. Total rainfall was measured using a tipping-bucket rain gauge. Individual rainfall events were defined by a cumulative rainfall depth exceeding 0.2 mm, separated by an inter-event dry period of at least 6 h [39,40]. The meteorological station collected data on rainfall, temperature (Temp), wind speed (Wind), wind direction (WD), atmospheric pressure (AP), and relative humidity (RH) at 1 min intervals. The evaporation variable (Evap) was obtained from a meteorological monitoring station located within the Jigongshan forest ecosystem encompassing the monitored catchments. The same station-based evaporation observations were used for all catchments to characterize the common background evaporative conditions of the study area. Throughfall was measured using rectangular collection troughs (1570 mm × 200 mm × 100 mm), which were installed on a 5° to 10° slope to direct the rainwater into a 50 mL automatic tipping collector [25,40]. Three collection troughs were randomly placed in each catchment, with their locations distributed within the monitored forest area to capture spatial variability in throughfall associated with heterogeneous canopy conditions. Three layers of mesh were installed above each collection trough to prevent clogging from leaves and debris. Stemflow was also measured in each catchment. Three trees were randomly selected in each catchment from the dominant tree species, *Quercus acutissima* and *Pinus massoniana*, for stemflow monitoring. A semicircular collar (inner diameter = 5 cm) was fixed to the edge of a 10 cm-wide weatherproof PVC tape, which was wrapped around the tree trunk at a height of 1.3 m. The collar directed stemflow to a 50 mL, ground-level tipping collector. The collar was fitted tightly against the trunk and sealed with silicone to prevent leaking. Real-time data were transmitted to an Internet of Things (IoT) platform via solar-powered wireless devices [33]. Because the canopy closure of the monitored mixed-forest catchments was approximately 90%, event-scale NP was calculated by considering both canopy-covered and open-gap areas. Rainfall reaching canopy-covered areas was represented by throughfall, whereas rainfall reaching open-gap areas was assumed to be equivalent to gross rainfall. Stemflow was added after being converted to an equivalent water depth per unit ground area. Before the formal monitoring period, canopy cover was visually estimated during vegetation surveys using the Braun–Blanquet phytosociological method. The estimated canopy cover values were 93%, 90%, and 88% for the three monitored mixed-forest catchments, respectively. Their mean canopy cover was approximately 90%; therefore, a representative value of $C = 0.9$ was adopted for all three catchments when calculating event-scale net precipitation. Therefore, event-scale NP was calculated as:

$$NP = Throughfall + (1 - C) \times Rainfall + Stemflow \quad (1)$$

where NP is event-scale net precipitation (mm), and C is canopy closure. For the studied catchments, C was 0.90.

2.2.2. Soil Moisture Monitoring

A multi-layer soil moisture monitoring system based on Frequency Domain Reflectometry (FDR) technology (JZ-LD1, Beijing Jiuzhou Shengxin Technology Co., Ltd., Beijing, China) was installed in each catchment, adjacent to the corresponding micro-meteorological station. The sensors were factory-calibrated before installation, and no additional site-specific calibration was performed. The system was vertically installed in boreholes perpendicular to the soil surface, and the borehole walls were smoothed to ensure effective coupling between the sensors and the soil. The continuous long-term measurements of this monitoring system began on 1 December 2023. Soil moisture data are recorded at 30 min intervals. Monitoring data are transmitted in real time to a cloud-based data management platform via a 4G IoT module. ISM was calculated as the thickness-weighted average volumetric water content across the 0–40 cm soil profile, based on four soil layers (0–10 cm, 10–20 cm, 20–30 cm and 30–40 cm). The calculation was performed as follows:

$$Wz = \frac{\sum_{i=0}^{n}(\theta i Di)}{\sum_{i=0}^{n} Di} \tag{2}$$

where Wz is the thickness-weighted volumetric soil moisture for the 0–40 cm soil profile, n is the number of soil layers (n = 4), θi is the volumetric water content of the i-th layer, and Di is the thickness of the i-th soil layer (cm).

For each rainfall event, ISM was computed using the soil moisture measured immediately before rainfall onset, representing ISM conditions prior to rainfall onset [35].

2.2.3. Runoff Monitoring and Hydrological Indices

To continuously monitor runoff dynamics, an integrated flow-gauging setup combining a notch weir and a Parshall flume was installed at the outlet of each catchment (Figure 1c). Within this combined structure, the notch weir collects and directs the runoff into the flume for accurate discharge measurements. The Parshall flume was used to monitor discharge based on changes in flow depth. In addition, an ultrasonic flow meter (JZ-LD1) was used for continuous monitoring of flow variation. This device measured flow in real time using a non-contact approach, improving the stability of high-frequency runoff measurements. All variables were recorded at 1 min intervals, including runoff depth, instantaneous discharge, water level, and flow velocity [8,11]. This setup allowed rapid changes in runoff during rainfall events to be effectively captured. Event runoff depth was automatically derived by the monitoring system from continuous discharge records and the predefined drainage area of each catchment. All monitoring data were transmitted in real time to a cloud-based data management platform via a 4G IoT module. Based on the monitoring data, the RC and SPD were calculated as follows:

$$RC = \frac{R}{NP} \tag{3}$$

where RC is the runoff coefficient, R is runoff depth (mm), and P is NP (mm).

Peak discharge was calculated as:

$$Peak\ discharge = max[Q(t)] \tag{4}$$

where $Q(t)$ is the real-time discharge at time t, and *Peak discharge* is defined as the maximum value of $Q(t)$ during a rainfall event.

$$SPD = \frac{Peak\ discharge}{A} \tag{5}$$

where SPD is the specific peak discharge [$m^3/(h \cdot km^2)$], and A is the catchment area (km^2).

2.3. Data Analysis and Statistical Methods

2.3.1. Random Forest Model Construction

The pooled dataset contained 81 event-catchment observations derived from 27 rainfall events recorded in the three monitored catchments. These events included all rainfall events during the monitoring period that satisfied the event separation criterion and had complete rainfall, soil moisture, and runoff observations. Previous hillslope and headwater catchment studies have analyzed datasets ranging from several tens to more than one hundred rainfall events [20,25], suggesting that the number of events included in the present study is within the range reported for comparable studies. For each rainfall event, observations from the three catchments were treated as separate catchment-level records and pooled into a single dataset for integrated RF analysis. Catchment identity was included as an explanatory variable to account for between-catchment differences. To avoid potential data leakage and dependence among observations from the same rainfall event, all catchment-level records associated with an individual rainfall event were assigned to the same subset when the dataset was divided into a training set (70%) and a testing set (30%), with a fixed random seed used to ensure reproducibility [41]. Environmental factors, including NP, RI, Wind, AP, Evap, and Temp, among others, together with catchment identity, were selected as input variables, while RC and SPD were used as output variables. The RF model was used to capture nonlinear relationships between environmental factors and the two-runoff metrics. The pooled dataset from the three monitored catchments was used to build a single RF model for each response variable. Model performance was evaluated using the coefficient of determination (R^2) and root mean square error (RMSE). The model showed robust simulation performance across all monitored catchments (Figure 2), indicating its effectiveness in capturing nonlinear hydrological responses during rainfall events. Further details on RF hyperparameters, event-level grouped data partitioning, and model evaluation are provided in Supplementary Method S1.

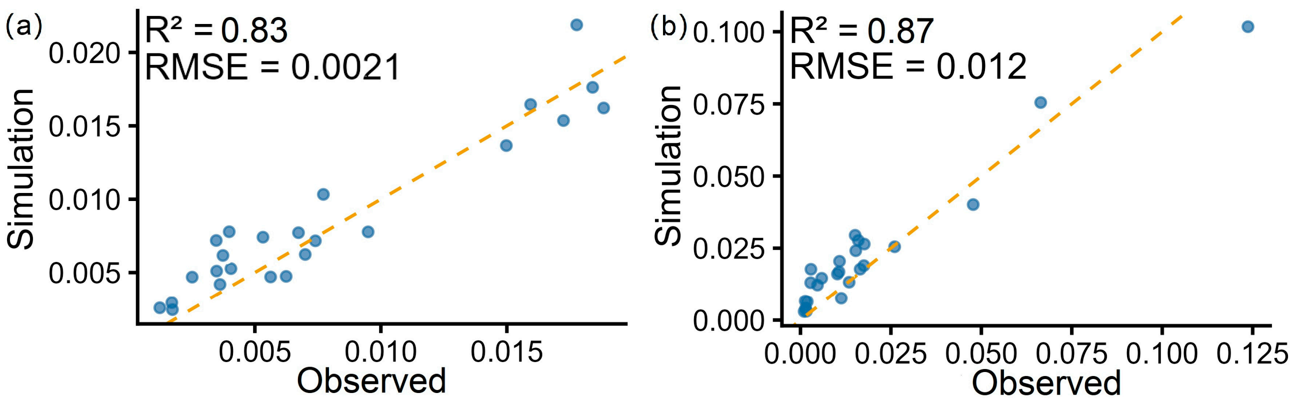

Figure 2. RF simulations of RC (**a**) and SPD (**b**). Blue dots indicate RF simulated values, and the orange dashed line indicates the 1:1 line between simulations and observations.

2.3.2. SHAP and PDPs for Model Interpretability

The RF model is widely regarded as a "black-box" model, which makes it difficult to explicitly reveal the relationships between environmental factors and runoff responses [29]. To address this limitation, SHAP was applied to interpret the RF model, as it quantifies the marginal contribution of environmental factors to runoff variability while avoiding the inherent bias toward nonlinear correlations found in traditional factor importance metrics, such as gain-based indices [42]. Based on cooperative game theory, SHAP decomposes model simulations into additive feature contributions, providing a detailed quantification of factor importance. To complement SHAP, partial dependence plots (PDPs) were used to show the average marginal effects of key environmental factors on model simulations. By marginalizing over the remaining features, PDPs were used to visualize the average marginal response of model predictions to selected input variables while recognizing that correlated predictors may influence interpretation. PDPs also facilitated identification of nonlinear response trends and potential interactions among variables. In ecohydrological applications, especially under data-limited conditions, PDPs provide an effective and interpretable tool for understanding model behavior.

2.3.3. Statistical Analyses

Pearson correlation analysis was first performed to examine pairwise correlations among all variables. The RF models were fitted in R using the "randomForest" package, while the results were visualized using "ggplot2". To interpret the RF model predictions and quantify the contributions of environmental factors to RC and SPD, SHAP values were calculated using "fastshap" and visualized using "shapviz". These analyses were used to characterize the importance and nonlinear contribution patterns of the explanatory variables. For each runoff metric, the ISM response threshold was identified from the SHAP dependence relationship as the approximate ISM value at which the contribution of ISM to the model prediction shifted from predominantly negative to predominantly positive. Subsequently, PDPs were generated from the fitted RF models to examine the average marginal effects of individual variables and explore the joint response patterns of pairs of variables. Two-dimensional partial dependence surfaces were visualized using "ggplot2" and "cowplot". Factor importance rankings and interaction matrices were organized using "dplyr" and plotted with "ggplot2". Based on the response-specific ISM thresholds, rainfall events were classified into below-threshold and above-threshold ISM groups separately for RC and SPD. The dominant factors and interaction patterns associated with each runoff metric were then analyzed separately under the two ISM states. All statistical analyses were conducted in the R environment(4.0.1).

3. Results

3.1. Characteristics of NP, ISM, RC, and SPD

During the study period, 27 rainfall events (383.65 mm in total) were recorded. The mean rainfall per event was 14.2 mm, with a maximum of 32.85 mm (Figure 3a). There were fourteen light (<10 mm) events, six moderate (10–25 mm) events, and seven heavy (>25 mm) events, contributing 21.8%, 24.1%, and 54.1% of the total rainfall, respectively. RI ranged from 0.52 to 4.33 mm h^{-1}, with a mean of 1.49 mm h^{-1}. RI < 1 mm h^{-1} occurred in 15 events, 1–3 mm h^{-1} occurred in 7 events, more than 3 mm h^{-1} occurred in 5 events. An RI of more than 3 mm h^{-1} contributed a total of 147.5 mm (38.4% of the total). The statistical distributions of ISM, RC, and SPD for rainfall events in catchments 1, 2, and 3 are shown in Figure 3b. ISM was highest in catchment 1, followed by catchments 3 and 2. Catchment 3 had higher median and mean RC values and a wider distribution range. Catchment 1 showed intermediate RC values with relatively large variability, whereas catchment 2 was characterized by overall lower and more concentrated RC values. SPD showed a pattern similar to that of RC. Catchment 3 had overall higher values and a longer upper whisker, whereas catchments 1 and 2 remained at lower levels with slight variability. Overall, catchment 3 exhibited the strongest runoff response, whereas catchment 2 showed the weakest response.

3.2. Correlations Among Environmental Factors, ISM, RC, and SPD

Pearson correlation analysis revealed a distinct correlation structure among antecedent wetness, rainfall characteristics, and runoff responses (Figure 4). The strongest association involving the runoff metrics was observed between ISM and SPD ($p < 0.001$), followed by that between ISM and RC ($p < 0.001$), indicating that both runoff metrics were closely associated with ISM, particularly SPD. RC and SPD were also positively correlated with each other ($p < 0.001$), while their correlations with rainfall-related variables showed broadly similar but not identical patterns. NP was positively correlated with RC, SPD, and ISM (all $p < 0.001$), whereas RI was positively correlated with RC ($p < 0.01$), SPD ($p < 0.001$), and ISM ($p < 0.001$). In contrast, Wind showed significant positive correlations with SPD ($p < 0.001$) and ISM ($p < 0.01$), but not with RC. Most other meteorological variables showed weak and nonsignificant linear correlations with RC and SPD. Overall, the correlation matrix highlights a closely associated group comprising ISM, NP, RI, RC, and SPD, while also revealing differences in the correlation patterns of RC and SPD with individual environmental variables.

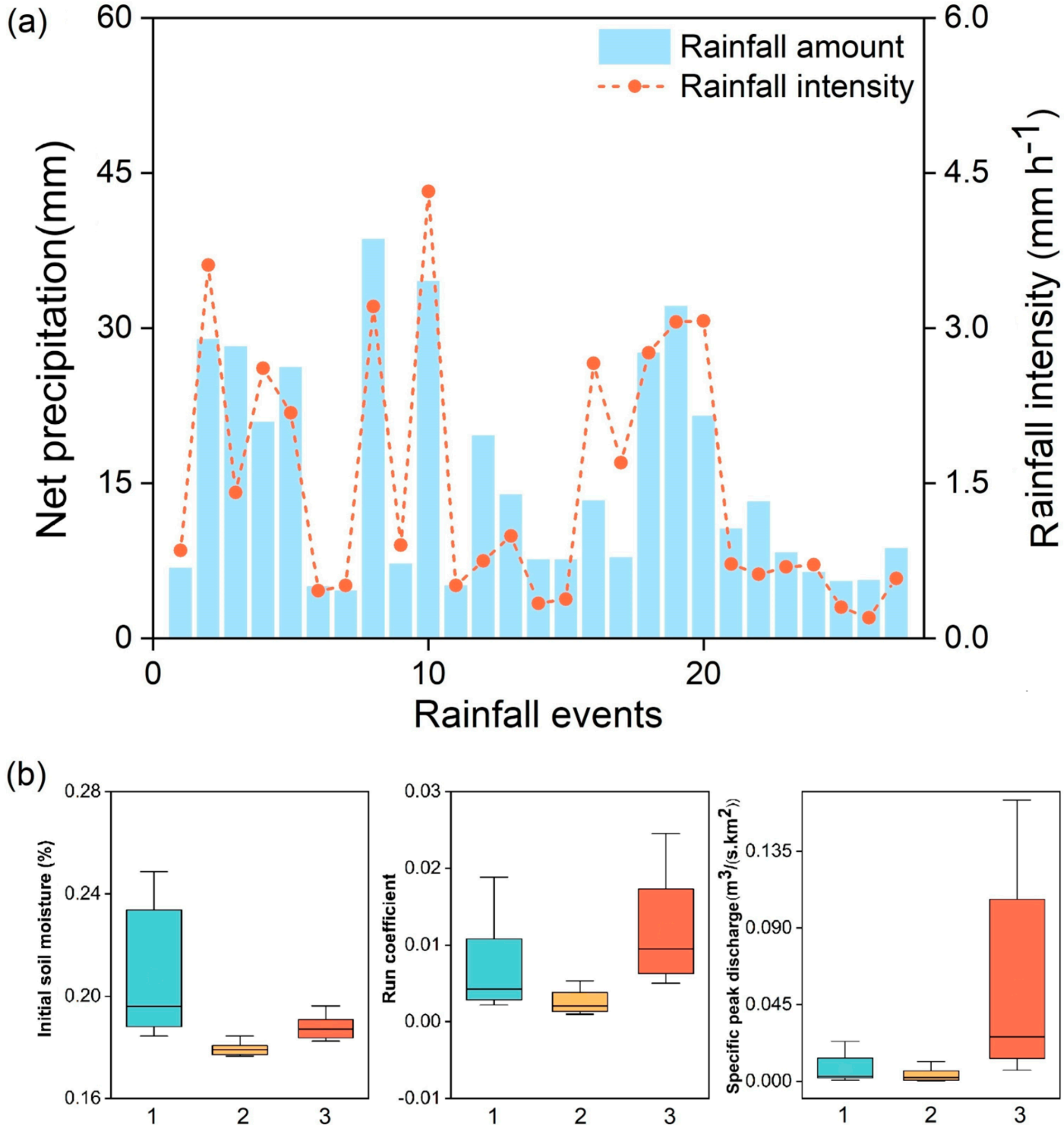

Figure 3. Net precipitation, rainfall intensity, initial soil moisture, RC, and SPD during the study period (**a**). ISM = initial soil moisture, RC = runoff coefficient, SPD = specific peak discharge (**b**), 1, 2, and 3 represent catchments 1, 2, and 3, respectively.

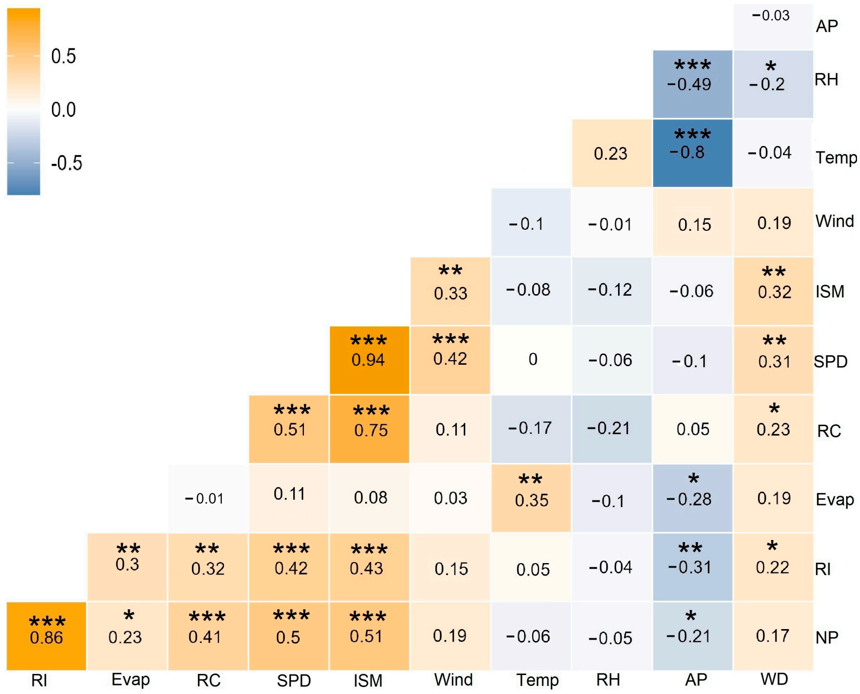

Figure 4. Pearson correlations among environmental factors, ISM, RC, and SPD. * $p < 0.05$, ** $p < 0.01$, *** $p < 0.001$, no * denotes not significant. NP = net precipitation, RI = rainfall intensity, Evap = evaporation, RC = runoff coefficient, SPD = specific peak discharge, ISM = initial soil moisture, Wind = wind speed, Temp = temperature, RH = relative humidity, AP = atmospheric pressure, WD = wind direction. Same abbreviations hereafter.

3.3. Individual Factor Effects on RC and SPD

The RF models demonstrated robust predictive performance, with R^2 values of 0.83 and 0.87 and corresponding RMSE values of 0.002 and 0.012, respectively. This predictive performance provided a reliable basis for interpreting the nonlinear hydrological responses using SHAP analysis (Figure 2). The importance rankings showed that ISM was the most important variable for both RC and SPD (Figure 5a,b). For RC, the three most important factors were ISM, NP, and Temp, whereas for SPD, they were ISM, NP, and RI. The third-ranked factor therefore differed between the two metrics, with RC showing stronger association with Temp and SPD showing stronger association with RI.

The SHAP beeswarm plots further illustrated the response patterns of the most influential predictors (Figure 5c,d). In the SHAP beeswarm plot, point color represents the observed value of each predictor, whereas the horizontal position represents its contribution to the model prediction relative to the baseline. Positive SHAP values indicate contributions that increase the predicted RC or SPD, whereas negative values indicate contributions that decrease the prediction. Thus, the clustering of high-ISM observations on the positive SHAP side means that higher observed ISM values were generally associated with positive contributions to the model-predicted runoff response. For RC, high ISM values were mainly associated with positive SHAP values, whereas low ISM values were mostly associated with negative SHAP values, indicating a positive contribution of higher ISM to RC. NP showed a similar pattern, with high values contributing mainly positively. In contrast, high Temp values were concentrated around zero or negative SHAP values, whereas some lower Temp values were associated with positive SHAP values. For SPD, the response patterns of ISM and NP were generally consistent with those of RC, with higher values mainly associated with positive SHAP values. In contrast to RC, RI showed a stronger influence on SPD, with high RI values concentrated in the positive SHAP range.

The difference between RC and SPD at the level of individual factors was therefore mainly reflected in the stronger contribution of Temp to RC and of RI to SPD.

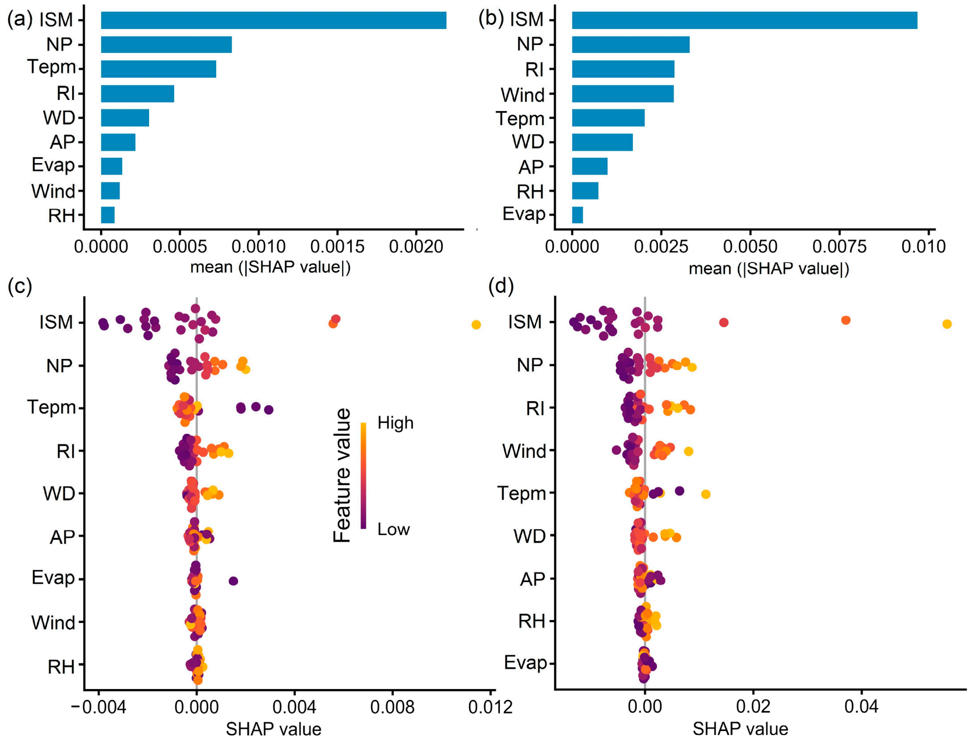

Figure 5. Importance ranking of individual factors and SHAP value distributions for RC and SPD: (**a**) importance ranking for RC, (**b**) importance ranking for SPD, (**c**) SHAP value distribution for RC, and (**d**) SHAP value distribution for SPD.

SHAP dependence plots showed that the SHAP values of different factors changed with factor values in different curve patterns, indicating that the responses of RC and SPD to different factors were not simply linear (Figure 6). Based on the above ranking of individual-factor importance, ISM was identified as a key factor influencing both RC and SPD, and its SHAP-based threshold behavior was therefore examined in more detail. As ISM increased, the SHAP values of both RC and SPD gradually increased from negative values and crossed zero. The zero-crossing point occurred at approximately 18.3% for RC and 19.2% for SPD, and the SHAP contribution of SPD increased more sharply beyond the threshold. These threshold values were used for the subsequent comparison of factor importance and interaction effects before and after the threshold.

3.4. Importance and Response Patterns of Factor Interactions

The interaction rankings showed that the leading interaction terms for both RC and SPD were centered on ISM (Figure 7). For RC, the three strongest interaction terms were NP × ISM, ISM × Temp, and ISM × RH (Figure 7a). For SPD, the three strongest interaction terms were NP × ISM, RI × ISM, and ISM × Wind (Figure 7b). NP × ISM ranked first for both RC and SPD. The interaction rankings also differed between RC and SPD: RC was mainly associated with interactions between ISM and meteorological variables, whereas SPD was more closely associated with interactions involving ISM and rainfall-related variables.

The PDPs further showed the response patterns of these dominant interaction terms (Figures 8 and 9). For RC, the NP × ISM interaction strengthened with increasing NP and ISM, and the ISM × Temp and ISM × RH interactions also increased under higher ISM conditions (Figure 8). For SPD, both NP × ISM and RI × ISM increased with ISM, whereas ISM × Wind increased with ISM over a smaller range (Figure 9).

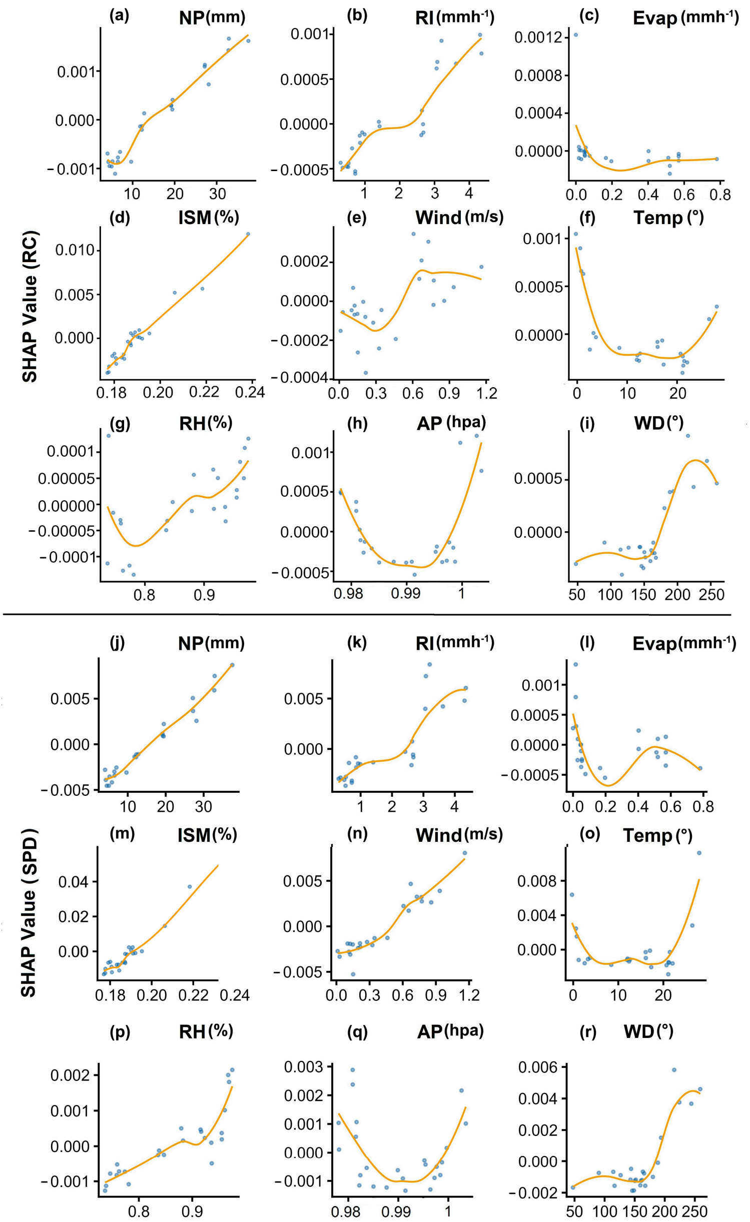

Figure 6. SHAP dependence plots of RC and SPD for individual factors. (**a**) NP for RC; (**b**) RI for RC; (**c**) Evap for RC; (**d**) ISM for RC; (**e**) Wind for RC; (**f**) Temp for RC; (**g**) RH for RC; (**h**) AP for RC; (**i**) WD for RC; (**j**) NP for SPD; (**k**) RI for SPD; (**l**) Evap for SPD; (**m**) ISM for SPD; (**n**) Wind for SPD; (**o**) Temp for SPD; (**p**) RH for SPD; (**q**) AP for SPD; (**r**) WD for SPD. Blue dots represent the SHAP values of individual samples, while the yellow lines indicate the fitted trends between each factor and its corresponding SHAP value.

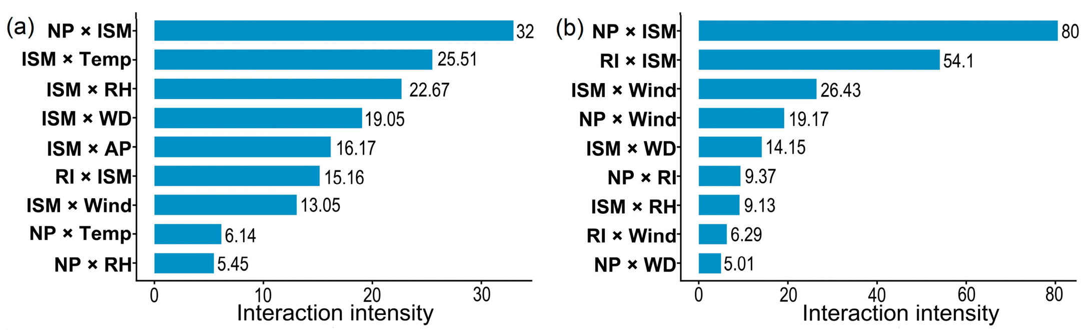

Figure 7. Importance ranking of interaction factors for RC and SPD. (**a**) RC and (**b**) SPD.

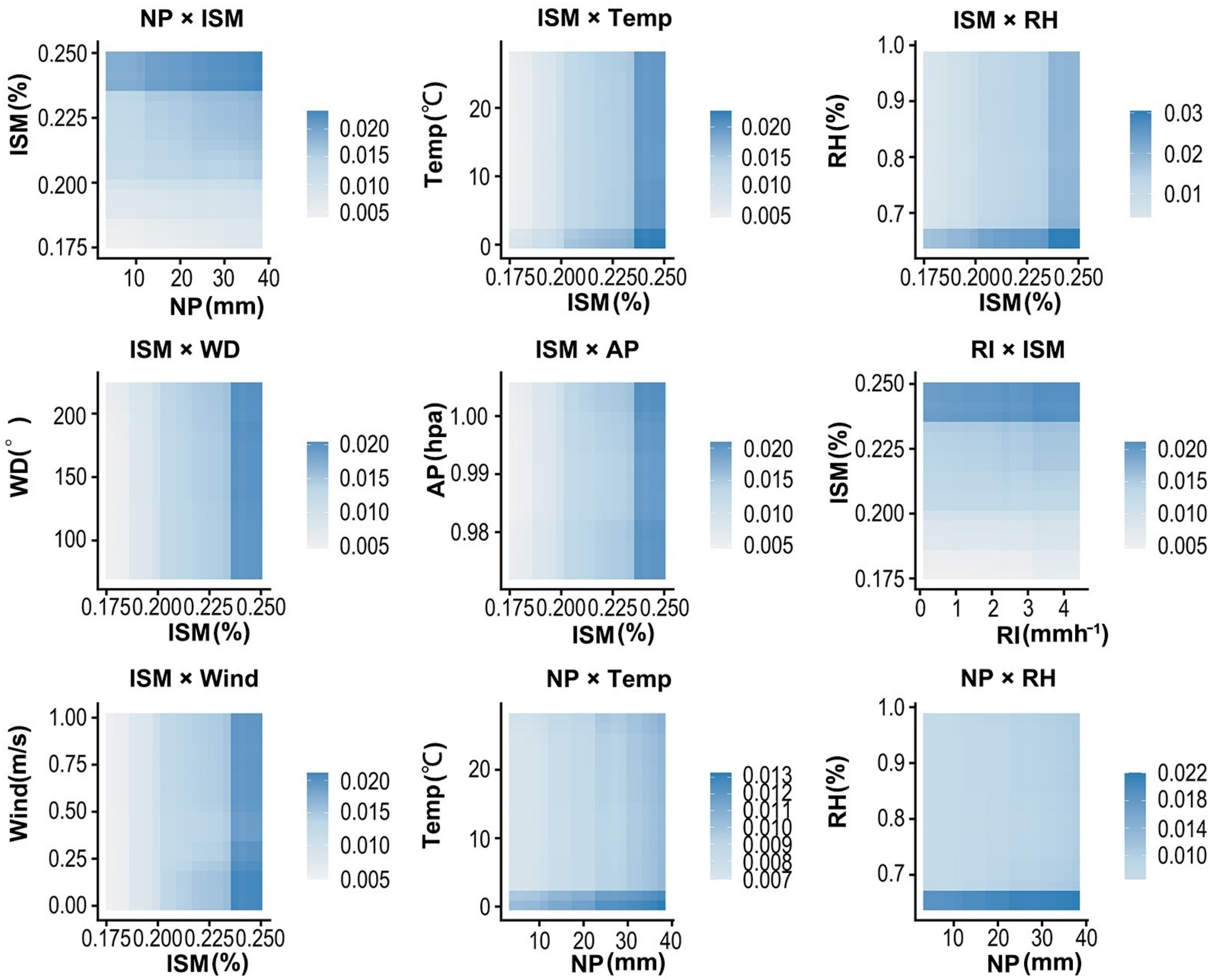

Figure 8. PDPs of RC for the main interaction factors.

3.5. Changes in Factor Importance and Interactions Based on the ISM Response Threshold

To investigate the state dependence of runoff controls, rainfall events were separately classified into pre-threshold and post-threshold states for RC and SPD based on the SHAP-derived ISM thresholds identified above (18.3% for RC and 19.2% for SPD). For RC, when ISM was below the threshold, the primary factors were ISM, RI, and NP (Figure 10a), and the leading interaction terms were RI × ISM and NP × ISM (Figure 11), both of which strengthened with increasing ISM. Conversely, when ISM exceeded the threshold, ISM remained the most important factor, while Temp and Evap increased to the second and third positions, and the importance of RI and NP decreased (Figure 10a). Concurrently, the dominant interactions shifted to Evap × ISM and ISM × AP, which also increased under wetter conditions (Figure 11). Regarding SPD, the dominant controls also showed clear differences between the two ISM states. When ISM was below the threshold, the main factors were RI, NP, and ISM (Figure 10b), and the dominant interactions were NP × RI and RI × ISM (Figure 12). By contrast, when ISM exceeded the threshold, ISM became the most important factor, followed by Wind and RI (Figure 10b). Correspondingly, the strongest interaction term shifted to ISM × Wind, and its effect increased with wind speed under higher ISM conditions (Figure 12). Meanwhile, the RI × ISM interaction remained important and showed a larger response range under higher ISM conditions (Figure 12).

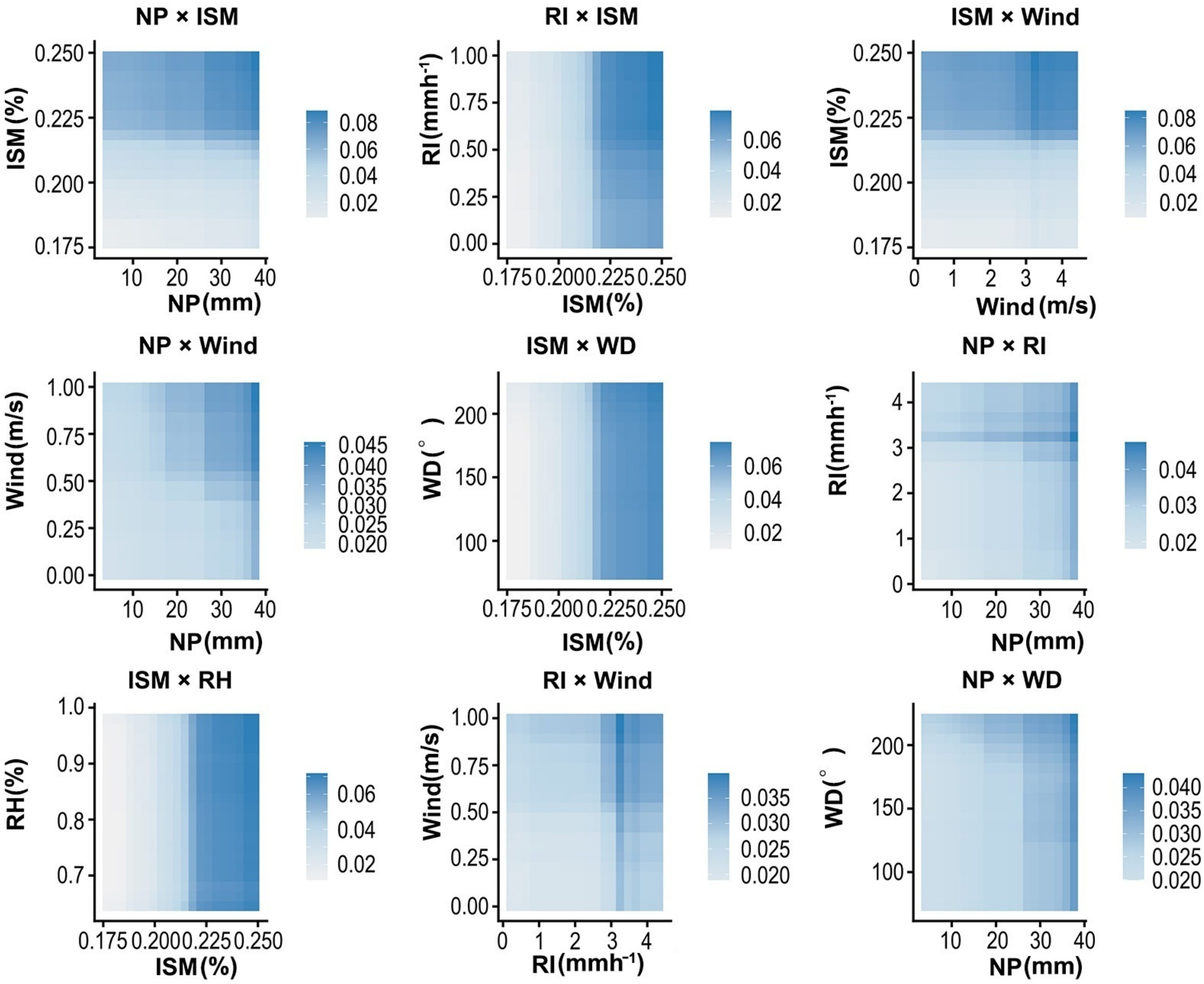

Figure 9. PDPs of SPD for the main interaction factors.

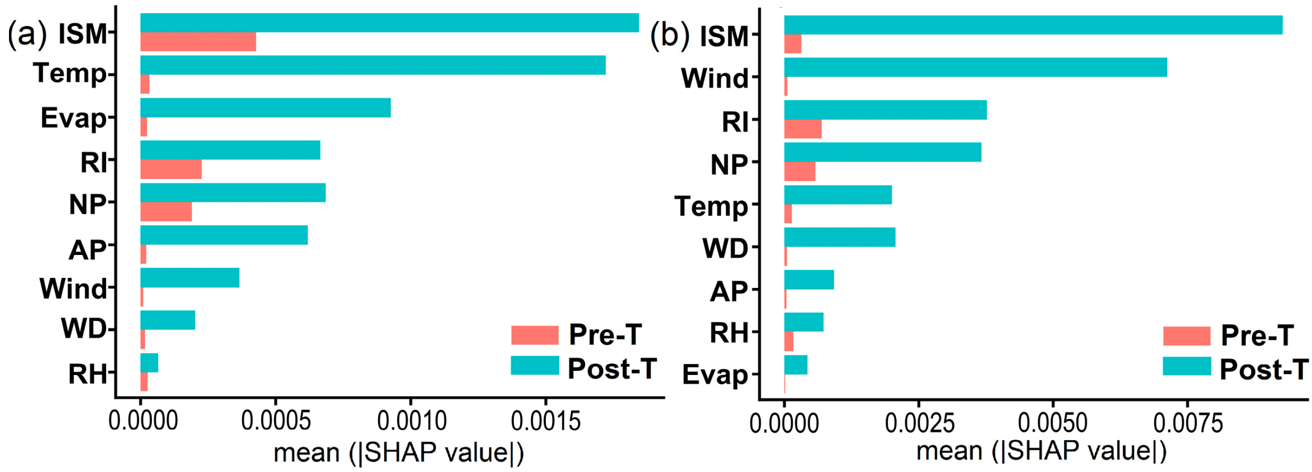

Figure 10. Changes in the importance ranking of individual factors across the ISM response threshold for RC and SPD: (**a**) RC and (**b**) SPD. Pre-T denotes the pre-threshold state, and post-T denotes the post-threshold state.

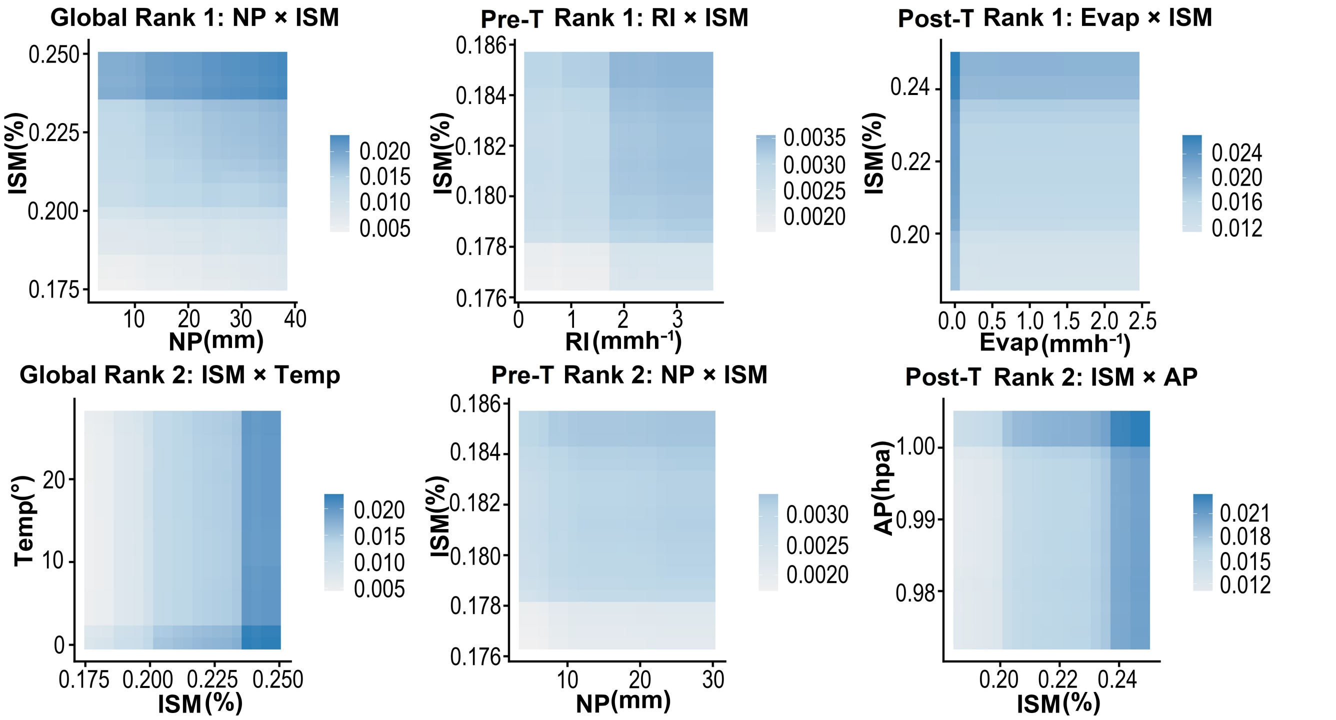

Figure 11. Changes in the interaction rankings and PDPs of RC across the ISM response threshold.

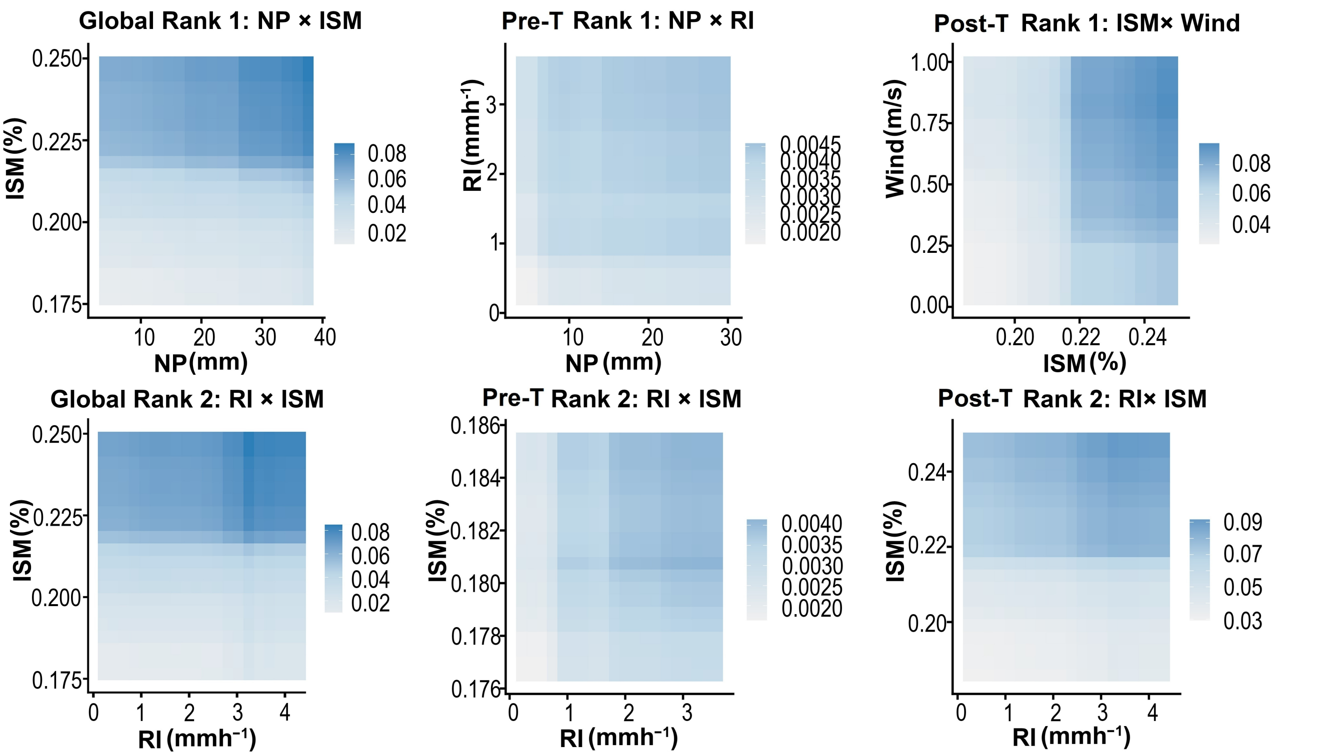

Figure 12. Changes in the interaction rankings and PDPs of SPD across the ISM response threshold.

4. Discussion

4.1. ISM Thresholds and State-Dependent Controls of Rainfall–Runoff Responses

Our results showed that event-scale runoff responses in the studied mixed-forest catchments were strongly associated with ISM. The higher ISM in catchment 1 and lower ISM in catchment 2 likely reflect differences in local soil properties and forest-site characteristics. Our previous study in the same area showed that soil organic carbon, particle-size composition, and soil pH were important factors associated with soil-moisture variability [35]. The Pearson correlation analysis confirmed the basic hydrological expectation that both RC and SPD were positively associated with ISM, NP, and RI (Figure 4). Building upon these linear relationships, the RF-SHAP analysis further revealed that the effects of the explanatory variables were nonlinear and that ISM was the dominant overall predictor for both RC and SPD across all event-catchment records (Figures 5 and 6). It should be emphasized that the RF-SHAP analysis identifies model-based statistical associations and predictor contributions rather than directly demonstrating the underlying runoff-generation mechanisms. Accordingly, the hydrological interpretations discussed below are considered plausible explanations supported by previous studies rather than causal mechanisms demonstrated by the present analysis. The dominant role of ISM is consistent with previous hydrological understanding that antecedent soil-water storage conditions influence the partitioning of incoming water between soil-water replenishment, infiltration, and runoff generation [30,43]. The high importance of NP is also consistent with the hydrological relevance of using canopy-modified effective water input in forested catchments, because canopy-modified rainfall components, including throughfall, stemflow, and direct rainfall in canopy gaps, determine the effective water input reaching the forest floor [33,34]. More broadly, the prominence of antecedent wetness and rainfall-related variables in the present models is qualitatively consistent with previous studies in forested catchments, which have identified antecedent soil moisture and rainfall characteristics as important controls on event-scale runoff responses [25,43,44].

A key finding is that the contribution of ISM to runoff responses exhibited clear nonlinear threshold behavior. The SHAP dependence plots showed that the contribution of ISM shifted from negative to positive at approximately 18.3% for RC and 19.2% for SPD (Figure 6). These thresholds should not be interpreted as fixed universal constants, but rather as model-derived diagnostic points that separate two contrasting antecedent wetness states in this catchment system [7,28]. Comparable nonlinear and threshold-dependent rainfall–runoff responses have been reported in previous catchment studies [20,23], and interpretable machine-learning studies have similarly identified nonlinear and site-dependent predictor–response relationships in hydrological systems [29,45]. However, direct numerical comparison of the ISM transition values among studies is not appropriate because such values may vary with catchment characteristics, soil-moisture monitoring depth, event definition, sample size, and model configuration. When ISM was below the threshold, the catchment was likely characterized by a substantial soil water storage deficit [8,16]. Under such conditions, rainfall inputs would first be consumed by soil-water replenishment, and hydrological connectivity among hillslope and channel components may remain relatively weak [18,26]. As a result, runoff generation and peak-discharge formation were more strongly constrained by the amount and intensity of rainfall required to overcome the antecedent storage deficit. When ISM exceeded the threshold, the catchment entered a wetter antecedent state in which available storage was substantially reduced. This condition is consistent with enhanced hydrological connectivity and a greater potential for saturation-related runoff responses or preferential flow activation [15,34].

4.2. State-Dependent Changes in Runoff Controls of RC and SPD

Differences in SHAP-based predictor importance and interaction strength between the pre-threshold and post-threshold groups are interpreted here as state-dependent changes in model associations rather than direct evidence of changes in runoff-generation mechanisms. Building on the ISM-state framework established above, the SHAP and PDP analyses showed that predictor rankings and interaction strengths for RC and SPD differed between the pre-threshold and post-threshold ISM states (Figures 10–12). This difference is expected because RC and SPD represent different aspects of event-scale runoff processes. RC reflects event-integrated rainfall–runoff conversion efficiency and is therefore closely related to available storage and atmospheric moisture-loss conditions [1,19]. By contrast, SPD represents short-duration peak-discharge formation and is more sensitive to rainfall intensity, water delivery rate, and rapid flow concentration processes [14,43].

For RC, the most influential predictors shifted from rainfall-related variables in the pre-threshold state to atmospheric and moisture-loss-related variables in the post-threshold state. When ISM was below the threshold, the leading factors were ISM, RI, and NP (Figure 10a), and the strongest interactions were RI × ISM and NP × ISM (Figure 11). Under these storage-deficit conditions, runoff conversion appeared to be primarily constrained by water availability [23,44]. Rainfall could be efficiently converted into runoff only when RI was sufficiently high to promote rapid runoff generation or when sufficient NP progressively filled the antecedent storage deficit [20,21]. The strong RI × ISM and NP × ISM interactions further show that the effect of rainfall input depended strongly on the antecedent wetness state. In the post-threshold state, ISM remained the most important factor for RC, but Temp and Evap increased to the second and third positions, while the importance of RI and NP decreased (Figure 10a). Once the catchment was already wet, additional rainfall supply appeared to become less strongly associated with variations in runoff conversion, whereas RC showed stronger associations with atmospheric conditions related to moisture loss and the partial recovery of soil storage capacity [45,46]. Higher evaporative demand may reduce soil moisture and partially restore the storage buffer, thereby affecting the proportion of subsequent effective water input converted into runoff [27,47]. The emergence of Evap × ISM as one of the strongest post-threshold interactions is consistent with this interpretation (Figure 11). The strong ISM × AP interaction should be interpreted cautiously. Rather than representing a direct runoff-generation mechanism, this model interaction may reflect broader synoptic meteorological conditions associated with wet-state runoff conversion [2,19]. Overall, the state-dependent change in RC was mainly expressed as a shift from stronger associations with rainfall-supply variables under drier conditions to stronger associations with moisture-loss and atmospheric-background variables under wetter conditions.

For SPD, the state-dependent changes differed from those of RC. In the pre-threshold state, the leading factors were RI, NP, and ISM, and the dominant interactions were NP × RI and RI × ISM (Figures 10b and 12). This pattern is consistent with peak-discharge formation under drier antecedent conditions being associated with both rainfall intensity and event water input. High RI alone may not produce a strong SPD response if NP is insufficient to overcome the storage deficit, whereas large NP with low RI may not generate rapid flow concentration efficiently [45,48]. Accordingly, pre-threshold SPD showed a combined association with rainfall forcing and antecedent storage conditions. In the post-threshold state, ISM became the most important factor for SPD, followed by Wind and RI (Figure 10b). Meanwhile, the strongest interaction shifted to ISM × Wind, while RI × ISM remained an important interaction with a larger response range under wetter conditions (Figure 12). Once antecedent storage deficits were reduced, SPD appeared to become less strongly associated with total water supply and more strongly associated with event-scale storm characteristics related to rapid water delivery and flow concentration [11,23]. The increased model importance of Wind in the post-threshold state is particularly noteworthy. Because direct observations of wind-driven rainfall redistribution, canopy shaking, or interception release were not available in this study, Wind should not be interpreted as an independent causal driver of runoff [44,45]. Wind may partly act as a proxy for storm type or broader synoptic meteorological conditions [24,47]. The strong ISM × Wind interaction indicates that, within the fitted model, the association between Wind and SPD varied with antecedent soil-moisture conditions, with windier events being associated with stronger SPD responses under wet antecedent conditions [4,30]. One possible hydrological interpretation is that wind may modify the spatial distribution and delivery of throughfall and stemflow in forested catchments [12,26]. Under wetter antecedent conditions, a reduced soil-storage buffer could potentially increase the sensitivity of peak discharge to such variations in effective water input. However, because these canopy-mediated processes were not directly measured, this interpretation remains hypothetical and cannot be distinguished from the possibility that Wind acts as a proxy for broader storm or synoptic conditions.

Overall, the predictor importance pattern for RC shifted from precipitation-related variables in the pre-threshold state toward evaporation- and atmospheric-condition-related variables in the post-threshold state. In contrast, SPD remained closely associated with RI and storm-event characteristics, while ISM and Wind showed greater model importance under wetter antecedent conditions. These results demonstrate that RC and SPD exhibited different state-dependent predictor-response patterns, supporting their separate consideration in event-scale rainfall–runoff analysis.

4.3. Implications and Limitations

The state-dependent runoff-control patterns identified above suggest that runoff responses may not be adequately represented by a single fixed parameterization across all antecedent wetness conditions. Instead, ISM may serve as a useful state variable for distinguishing contrasting runoff-response regimes. Accordingly, state-dependent parameter schemes or threshold-informed model structures may provide a useful direction for improving event-scale runoff simulation in mixed-forest catchments [4,10].

For conceptual or semi-distributed models such as TOPMODEL, HBV, or the Xin'anjiang model, the ISM threshold identified in this study could be used as a diagnostic reference for adjusting storage-related parameters or runoff response functions. For example, pre-threshold events may require model structures that emphasize soil-water replenishment and larger effective storage capacity, whereas post-threshold events may require stronger representation of reduced storage capacity, enhanced runoff connectivity, and faster response to storm forcing. However, these implications should be treated as hypotheses for model development rather than as directly validated parameterization rules. Future modeling studies are needed to determine whether separate calibration, state-dependent parameter adjustment, or threshold-based runoff response functions improve event-scale simulation compared with a single parameter set applied across all ISM states [43,48]. The ISM transition range identified in this study, approximately 18%–19%, may provide a site-specific reference for evaluating runoff responses in this mixed-forest region. When monitored ISM approaches or exceeds this range, stronger runoff responses may become more likely, particularly when subsequent rainfall is characterized by high RI, sufficient NP, or windier storm conditions. Combining ISM with RI, NP, and Wind may therefore help identify rainfall events with greater potential for rapid runoff responses [46,49]. Nevertheless, this threshold should not be used as a deterministic warning criterion or as a standalone decision basis. Runoff responses are also influenced by rainfall duration and temporal distribution, canopy wetness and interception dynamics, spatial variability in throughfall and stemflow, soil properties, and catchment heterogeneity. Therefore, the threshold is more appropriately used as a supplementary indicator within a broader monitoring and assessment framework. Future work should further evaluate its reliability using longer-term real-time ISM observations and independent rainfall–runoff events.

This study also has several limitations that should be considered when interpreting the results. First, the analysis was based on three sub-catchments within a single mixed-forest watershed and a limited number of rainfall events. Although pooling event-catchment records supported the RF-SHAP analysis, the identified ISM thresholds may still be influenced by local climate, vegetation structure, soil texture, topography, and monitored soil depth. Therefore, multi-year and multi-site validation is needed before these threshold values can be generalized to other forested catchments [36,42]. Second, the RF-SHAP framework identifies statistical contributions and interaction patterns rather than direct causal evidence of runoff pathways. Thus, the inferred enhancement of hydrological connectivity and saturation-related runoff responses under wetter conditions should be further tested using tracer experiments, soil moisture profile observations, shallow groundwater monitoring, and subsurface flow measurements [9,17]. In particular, the interpretations of Wind and AP should be regarded as plausible but not yet directly verified mechanisms. Future research should integrate event-scale interpretable machine learning with field hydrological observations and process-based modeling to evaluate whether SHAP-derived ISM thresholds correspond to measurable changes in soil water storage, hydrological connectivity, and runoff response behavior. Such integration would allow the threshold concept to be assessed not only as a statistical diagnostic tool, but also as a process-informed framework for improving rainfall–runoff simulation and runoff-risk assessment in mixed-forest catchments [37,50].

5. Conclusions

This study examined the nonlinear role of ISM in event-scale rainfall–runoff responses in mixed-forest catchments using RF, SHAP, and PDP analyses. ISM was the dominant predictor of both RC and SPD, while NP played an important role as canopy-modified effective water input. The strong NP × ISM interaction indicates that runoff responses depended on the coupling between effective rainfall input and antecedent wetness conditions. SHAP dependence analysis identified ISM thresholds of approximately 18.3% for RC and 19.2% for SPD, where the contribution of ISM to RF predictions changed from negative to positive. These thresholds should be interpreted as model-derived transition points separating contrasting antecedent wetness states, rather than directly observed physical saturation thresholds. Dominant factors and interaction structures differed between pre-threshold and post-threshold ISM states. For RC, the main secondary controls changed from RI and NP to Temp and Evap, with leading interactions changing from RI × ISM and NP × ISM to Evap × ISM and ISM × AP. For SPD, RI and NP were more important in the pre-threshold state, whereas ISM, Wind, and RI became more influential in the post-threshold state, accompanied by a change from NP × RI and RI × ISM to ISM × Wind and RI × ISM. These findings highlight the need to incorporate ISM thresholds, NP, and state-dependent runoff controls into event-scale runoff modeling in mixed-forest catchments.

Supplementary Materials: The following supporting information can be downloaded at: https://www.mdpi.com/article/10.3390/f17080986/s1, Supplementary Method S1: Random Forest implementation details; Supplementary Method S2: Model performance metrics; Table S1: Descriptive statistics of NP, ISM, RC, and SPD in the three monitored catchments.

Author Contributions: Conceptualization, Q.Z. and S.D.; methodology, Y.M.; software, D.W.; validation, Y.M., T.W. and L.Z.; formal analysis, Y.M.; investigation, Y.M., D.W., T.W. and L.Z.; resources, Y.M.; data curation, Y.M.; writing—original draft preparation, Y.M.; writing—review and editing, Q.Z.; visualization, Y.M.; supervision, Q.Z. and S.D.; project administration, Q.Z. and S.D.; funding acquisition, Q.Z. and S.D. All authors have read and agreed to the published version of the manuscript.

Funding: This research was funded by the National Natural Science Foundation of China (41971229), Natural Science Foundation of Henan (262300421049), and Xinyang Academy of Ecological Research Open Foundation (2023XYZD03, 2023DBS01).

Data Availability Statement: Data will be made available on request.

Acknowledgments: We would like to extend our sincere gratitude to all our research group members for their indispensable contributions to the data collection process. Their commitment and diligent efforts were fundamental to the successful realization of this study.

Conflicts of Interest: The authors declare no conflicts of interest.

References

1. Kameyama, T.; Kumagai, T.; Egusa, T.; Momiyama, H. Importance of bedrock hydrology for the rainfall-runoff process in a forested mountain catchment. *J. Hydrol.* **2026**, *664*, 134205. [CrossRef]
2. Penna, D. Controls on runoff processes in forested catchments worldwide. *Nat. Water* **2026**, *4*, 102–114. [CrossRef]
3. Fischer, S.; Moderow, U.; Queck, R.; Bernhofer, C. Evaporation of intercepted rainfall-comparing canopy water budget and energy balance related long term measurements at a Norway spruce site. *Agric. For. Meteorol.* **2023**, *341*, 109637. [CrossRef]
4. Lan, T.; Zhang, J.; Cheng, W.; Wang, X.; Zhang, H.; Gong, X.; Xie, X.; Chen, Y.; Xu, C. A robust calibration and evaluation framework for dynamic catchment characteristics in hydrological modeling. *Hydrol. Earth Syst. Sci.* **2026**, *30*, 2455–2471. [CrossRef]
5. Ding, B.; Yu, X.; Jia, G. Exploring the controlling factors of watershed streamflow variability using hydrological and machine learning models. *Water Resour. Res.* **2025**, *61*, e2024WR039734. [CrossRef]
6. Zhou, J.; Wen, Y.; Gao, P.; Ren, S.; Guo, X.; Mu, X. Transitions in slope runoff generation mechanisms induced by land use change in the Loess Plateau, China. *Catena* **2025**, *261*, 109517. [CrossRef]
7. Liu, S.; Seybold, H.; van Meerveld, I.; Wang, Y.; Kirchner, J.W. Tree planting and soil conservation measures have strongly attenuated storm runoff responses on the Chinese Loess Plateau. *J. Hydrol.* **2025**, *662*, 134039. [CrossRef]
8. Xu, Z.; Jiang, B.; Guo, X.; Wu, Z.; Fan, S. Initial soil moisture conditions dominate variation in event-scale propagation time from meteorological to agricultural drought. *Agric. Water Manag.* **2026**, *325*, 110128. [CrossRef]
9. Kojima, N.; Tani, M. Evaluating effects of catchment properties and antecedent moisture conditions on storm runoff responses based on hillslope observations in a small mountainous catchment. *J. Hydrol.* **2025**, *660*, 133464. [CrossRef]
10. Yang, W.; Li, C.; Yang, H. Impacts of spatial-temporal rainfall structures and antecedent wetness on flood variability at the catchment scale. *J. Hydrol.* **2026**, *669*, 135019. [CrossRef]
11. Liu, Y.; Long, Y.; Lei, M.; Li, T.; Zeng, Q.; Yin, Y.; Sun, G.; Ma, Y.; Xiao, P.; Ye, J.; et al. Nonlinear responses between watershed hydrological functional connectivity and rainfall-runoff-sediment. *Water Resour. Res.* **2026**, *62*, e2025WR042706. [CrossRef]
12. Xiong, T.; Tian, J.; Niu, B.N.; Wang, Y.; Xiang, H.; Huang, H.; Kang, W.; Zhang, B.; He, C. Soil moisture response to rainfall and its controls on hillslopes in alpine mountain areas of the Tibetan Plateau. *J. Hydrol.* **2026**, *664*, 134425. [CrossRef]
13. Li, H.; Huang, Y.; Qi, Y.; Jiang, Y.; Tang, X.; Boyer, E.W.; Mello, C.R.; Lan, P.; Guo, L. Improved streamflow simulation by assimilating in situ soil moisture in lumped and distributed approaches of a hydrological model in a headwater catchment. *Water Resour. Manag.* **2024**, *38*, 4933–4953. [CrossRef]
14. Qi, Y.; Fan, B.; Zhang, Y.; Jiang, Y.; Huang, Y.; Boyer, E.W.; Mello, C.R.; Guo, L.; Li, H. Estimating root zone soil moisture using the SMAR model and regression method at a headwater catchment with complex terrain. *Geoderma* **2025**, *453*, 117144. [CrossRef]
15. Sun, J.; Yang, K.; He, X.; Wang, G.; Wang, Y.; Yu, Y.; Lu, H. Causal pathways underlying global soil moisture-precipitation coupling. *Nat. Commun.* **2025**, *16*, 8935. [CrossRef] [PubMed]
16. Zwartendijk, B.W.; van Meerveld, H.J.; Ghimire, C.P.; Bruijnzeel, L.A.; Ravelona, M.; Jones, J.P.G. Rebuilding soil hydrological functioning after swidden agriculture in eastern Madagascar. *Agric. Ecosyst. Environ.* **2017**, *239*, 101–111. [CrossRef]
17. Yang, Y.; Yang, L.; Villarini, G.; Zhao, F.; Huang, D.; Vecchi, G.A.; Wang, Q.; Sun, Y.; Tian, F. Synchronization of global peak river discharge since the 1980s. *Nat. Clim. Change* **2025**, *15*, 1084–1090. [CrossRef]
18. Xiao, X.; Zhang, F.; Che, T.; Shi, X.; Zeng, C.; Wang, G.; Liu, J.; Wu, H.; Liu, K.; Yu, Z.; et al. Changes in plot-scale runoff generation processes from the spring-summer transition period to the summer months in a permafrost-dominated catchment. *J. Hydrol.* **2020**, *587*, 124966. [CrossRef]
19. Wu, Q.; Xie, T.; Liu, C.; Li, W.; Zhang, L.; Ran, G.; Xu, Y.; Tang, Y.; Han, Z.; Hu, C. Improving the understanding of rainfall-runoff processes: Temporal dynamic of event runoff response in Loess Plateau, China. *J. Environ. Manag.* **2025**, *375*, 123436. [CrossRef] [PubMed]
20. Lee, E.; Kim, S. Characterization of runoff generation in a mountainous hillslope according to multiple threshold behavior and hysteretic loop features. *J. Hydrol.* **2020**, *590*, 125534. [CrossRef]
21. Buechel, M.; Slater, L.; Dadson, S. Hydrological impact of widespread afforestation in Great Britain using a large ensemble of modelled scenarios. *Commun. Earth Environ.* **2022**, *3*, 6. [CrossRef]
22. Nakai, T.; Lai, Y. Micrometeorological estimation of wet canopy evaporation from a cloud forest in central Taiwan. *Agric. For. Meteorol.* **2024**, *350*, 109997. [CrossRef]

23. Wang, S.; Yan, Y.; Fu, Z.; Chen, H. Rainfall-runoff characteristics and their threshold behaviors on a karst hillslope in a peak-cluster depression region. *J. Hydrol.* **2022**, *605*, 127370. [CrossRef]
24. Zhang, G.; Tang, D.; Li, S.; Fan, Y.; Pulatov, A.; Sun, A.; Qi, X.; Wang, L.; Li, Y. Climate and land use regulate vegetation-runoff interaction pathways in the three-river source region. *J. Environ. Manag.* **2025**, *393*, 127127. [CrossRef] [PubMed]
25. Singh, N.K.; Emanuel, R.E.; McGlynn, B.L.; Miniat, C.F. Soil Moisture Responses to Rainfall: Implications for Runoff Generation. *Water Resour. Res.* **2021**, *57*, e2020WR028827. [CrossRef]
26. Zhu, H.; Chen, Y.; Huang, Z. Quantifying the runoff generation mechanisms response to vegetation restoration in the Loess Plateau in China: A novel dual-index identification framework integrated with multinomial logistic regression. *J. Hydrol.* **2026**, *664*, 134480. [CrossRef]
27. Feng, H.; Zhou, J.; Wu, Z.; Dong, J.; Brocca, L.; Zhao, L.; He, H.; Fan, H. Optimizing soil moisture-runoff coupling strength with remotely sensed soil moisture for improved hydrological modeling. *Water Resour. Res.* **2026**, *62*, e2024WR039571. [CrossRef]
28. Fischer-Bedtke, C.; Metzger, J.C.; Demir, G.; Wutzler, T.; Hildebrandt, A. Throughfall spatial patterns translate into spatial patterns of soil moisture dynamics-empirical evidence. *Hydrol. Earth Syst. Sci.* **2023**, *27*, 2899–2918. [CrossRef]
29. Fu, X.; Wang, M.; Zhang, D.; Chen, F.; Peng, X.; Wang, L.; Tan, S.K. An XGBoost-SHAP framework for identifying key drivers of urban flooding and developing targeted mitigation strategies. *Ecol. Indic.* **2025**, *175*, 113579. [CrossRef]
30. Kan, F.; Lian, X.; Xu, H.; Tang, S.; Cui, J.; Huntingford, C.; Sun, M.; Li, X.; Piao, S. Latitudinal divergence in runoff responses to global forestation due to forest-atmosphere feedbacks. *Nat. Commun.* **2026**, *17*, 2515. [CrossRef] [PubMed]
31. Nguyen, T.; Bennett, B.; Leonard, M. Tracking rainfall contribution in a conceptual runoff model. *J. Hydrol.* **2026**, *672*, 135366. [CrossRef]
32. Panahandeh, T.; Attarod, P.; Sadeghi, S.M.M.; Bayramzadeh, V.; Tang, Q.; Liu, X. The performance of the reformulated Gash rainfall interception model in the Hyrcanian temperate forests of northern Iran. *J. Hydrol.* **2022**, *612*, 128092. [CrossRef]
33. Niu, X.; Fan, J.; Du, M.; Dai, Z.; Luo, R.; Yuan, H.; Zhang, S. Changes of rainfall partitioning and canopy interception modeling after progressive thinning in two shrub plantations on the Chinese Loess Plateau. *J. Hydrol.* **2023**, *619*, 129299. [CrossRef]
34. Yang, J.; He, Z.; Feng, J.; Lin, P.; Du, J.; Guo, L.; Liu, Y.; Yan, J. Rainfall interception measurements and modeling in a semiarid evergreen spruce (*Picea crassifolia*) forest. *Agric. For. Meteorol.* **2023**, *328*, 109257. [CrossRef]
35. Mei, Y.; Zhao, Q.; Li, P.; Qin, X.; Liu, B.; Li, Z.; Wang, T.; Ding, S. Soil moisture variability of typical mixed forests in the north-south climatic transitional zone of China. *J. Environ. Manag.* **2025**, *395*, 127953. [CrossRef] [PubMed]
36. Yu, J.; Zhao, Q.; Ding, S.; Yu, Z.; Liu, Y. Gully development drives sediment transport efficiency of forest road-stream pathways in mountainous watershed. *Catena* **2025**, *258*, 109229. [CrossRef]
37. Zhao, Q.; Wang, A.; Yu, Z.; Yu, J.; Liu, Y.; Zhang, G.; Liu, G.; Wang, P.; Ding, S. Factors contributing to rill erosion of forest roads in a mountainous watershed. *J. Environ. Manag.* **2023**, *326*, 116829. [CrossRef] [PubMed]
38. Yu, Z.; Zhao, Q.; Ding, S.; Yu, J.; Liu, B.; Feng, W.; Li, Y.; Zhou, J. Unpaved road-altered confluence networks exacerbate soil organic carbon loss in mountainous forested catchments. *J. Hydrol.* **2026**, *664*, 134500. [CrossRef]
39. de Carvalho Lopes, D.; Steidle Neto, A.J.; de Queiroz, M.G.; de Souza, L.S.B.; Zolnier, S.; da Silva, T.G.F. Sparse Gash model applied to seasonal dry tropical forest. *J. Hydrol.* **2020**, *590*, 125497. [CrossRef]
40. Ma, M.; Li, Q.; Wang, Y.; Liang, J.; Wang, J.; Liu, J.; Zhang, M. Rainfall intensities determine accuracy of canopy interception simulation using the revised Gash model. *Agric. For. Meteorol.* **2025**, *362*, 110389. [CrossRef]
41. Li, P.; Ding, S.; Xin, X.; Zhu, A.; Ding, S.; Mei, Y.; Liu, Y.; Wu, X.; Lu, K.; Zhao, Q. Ecological niche differentiation of detritivores dominates soil mesofaunal community assembly in a 33-year fertilized cropland. *Soil Till. Res.* **2025**, *252*, 106605. [CrossRef]
42. Ren, X.; Li, G.; Sun, X.; He, H.; Zhao, Q.; Wang, L.; Gong, Y.; Han, B.; Cao, C. Opposite responses of water use efficiency and carbon use efficiency to agricultural drought during winter wheat growth period in the core area of grain production in the ancient course of Yellow River. *Agric. Water Manag.* **2026**, *324*, 110144. [CrossRef]
43. Nanda, A.; Safeeq, M. Threshold controlling runoff generation mechanisms in Mediterranean headwater catchments. *J. Hydrol.* **2023**, *620*, 129532. [CrossRef]
44. Nanda, A.; Sen, S.; McNamara, J.P. How spatiotemporal variation of soil moisture can explain hydrological connectivity of infiltration-excess dominated hillslope: Observations from lesser Himalayan landscape. *J. Hydrol.* **2019**, *579*, 124146. [CrossRef]
45. Meli, P.; Ellison, D.; Ferraz, S.F.d.B.; Filoso, S.; Brancalion, P.H.S. On the unique value of forests for water: Hydrologic impacts of forest disturbances, conversion, and restoration. *Glob. Change Biol.* **2024**, *30*, e17162. [CrossRef]
46. Felton, A.J.; Fisher, J.B.; Hufkens, K.; Purdy, A.J.; Spawn-Lee, S.A.; Duloisy, L.F.; Goldsmith, G.R. Global estimates of the storage and transit time of water through vegetation. *Nat. Water* **2025**, *3*, 59–69. [CrossRef]
47. Liu, S.; Kirchner, J.; Slater, L.J.; Floriancic, M.G.; Van Meerveld, I.; Berghuijs, W.R. Forest Impacts on peak runoff revealed by accounting for the effects of climate. *Geophys. Res. Lett.* **2026**, *53*, e2025GL121139. [CrossRef]
48. Brandao, A.R.A.; Husic, A.; Almagro, A.; Schwamback, D.; Oliveira, P.T.S. Explaining spatial variation and catchment characteristics thresholds in streamflow response. *J. Hydrol.* **2026**, *674*, 135492. [CrossRef]

49. Brasil, J.B.; de Andrade, E.M.; Guerreiro, M.S.; Palácio, H.A.d.Q.; Ribeiro Filho, J.C.; Fernández-Raga, M.; Medeiros, P.H.A. Measurement and modelling of kinetic energy and erosivity of rainfall and throughfall in a tropical semiarid region. *J. Hydrol.* **2024**, *644*, 132088. [CrossRef]
50. Zhang, H.; Zhang, Y.; Miralles, D.G.; Tai, X.; Koppa, A.; Yang, H.; Sitch, S.; O'Sullivan, M. Increase in plant reliance on past precipitation associated with greening and drying. *Nat. Ecol. Evol.* **2026**, *10*, 689–699. [CrossRef] [PubMed]